The Astrophysical Journal Letters, 961:L25 (9pp), 2024 January 20 https://doi.org/10.3847/2041-8213/ad11ee

Uncovering a Massive $z \sim 7.7$ Galaxy Hosting a Heavily Obscured Radio-loud Active Galactic Nucleus Candidate in COSMOS-Web

Erini Lambrides[1,40], Marco Chiaberge[2,3], Arianna S. Long[4,41], Daizhong Liu[5], Hollis B. Akins[4], Andrew F. Ptak[1], Irham Taufik Andika[5,6], Alessandro Capetti[7], Caitlin M. Casey[4,8], Jaclyn B. Champagne[9], Katherine Chworowsky[4,42], Tracy E. Clarke[10], Olivia R. Cooper[4,42], Xuheng Ding[11], Dillon Z. Dong[12], Andreas L. Faisst[13], Jordan Y. Forman[14,15], Maximilien Franco[4], Steven Gillman[8,16], Ghassem Gozaliasl[17,18], Kirsten R. Hall[19], Santosh Harish[20], Christopher C. Hayward[21], Michaela Hirschmann[22,23], Taylor A. Hutchison[1,41], Knud Jahnke[24], Shuowen Jin[8,16,43], Jeyhan S. Kartaltepe[20], Emma T. Kleiner[14,15], Anton M. Koekemoer[2], Vasily Kokorev[25], Sinclaire M. Manning[26,41], Crystal L. Martin[27], Jed McKinney[4], Colin Norman[2,3], Kristina Nyland[10], Masafusa Onoue[11,28], Brant E. Robertson[29], Marko Shuntov[30,31], John D. Silverman[32,33], Massimo Stiavelli[2], Benny Trakhtenbrot[34], Eleni Vardoulaki[35], Jorge A. Zavala[36], Natalie Allen[30,31], Olivier Ilbert[37], Henry Joy McCracken[38], Louise Paquereau[38], Jason Rhodes[39], and Sune Toft[30,31]

[1] NASA-Goddard Space Flight Center, Code 662, Greenbelt, MD 20771, USA; erini.lambrides@nasa.gov
[2] Space Telescope Science Institute, 3700 San Martin Drive Baltimore, MD 21218, USA
[3] Department of Physics & Astronomy, Johns Hopkins University, Bloomberg Center, 3400 N. Charles Street, Baltimore, MD 21218, USA
[4] Department of Astronomy, The University of Texas at Austin, 2515 Speedway Boulevard Stop C1400, Austin, TX 78712, USA
[5] Max-Planck-Institut für Astrophysik, Karl-Schwarzschild-Str. 1, D-85748 Garching, Germany
[6] Technical University of Munich, TUM School of Natural Sciences, Department of Physics, James-Franck-Str. 1, D-85748 Garching, Germany
[7] INAF Osservatorio Astrofisico di Torino, Strada Osservatorio 20, I-10025 Pino Torinese, Italy
[8] Cosmic Dawn Center (DAWN), Denmark
[9] Steward Observatory, University of Arizona, 933 N Cherry Avenue, Tucson, AZ 85721, USA
[10] U.S. Naval Research Laboratory, 4555 Overlook Avenue SW, Washington, DC 20375, USA
[11] Kavli Institute for the Physics and Mathematics of the Universe (Kavli IPMU, WPI), The University of Tokyo, Chiba 277-8583, Japan
[12] National Radio Astronomy Observatory, 1003 Lopezville Road, Socorro, NM 87801, USA
[13] Caltech/IPAC, MS 314-6, 1200 E. California Boulevard, Pasadena, CA 91125, USA
[14] Southeastern Universities Research Association, Washington DC, USA
[15] NASA Goddard Space Flight Center, Greenbelt, MD 20771, USA
[16] DTU-Space, Technical University of Denmark, Elektrovej 327, DK-2800 Kgs. Lyngby, Denmark
[17] Department of Computer Science, Aalto University, P.O. Box 15400, Espoo, FI-00076, Finland
[18] Department of Physics, University of Helsinki, P.O. Box 64, FI-00014, Helsinki, Finland
[19] Radio & Geoastronomy Division, Center for Astrophysics | Harvard & Smithsonian, 60 Garden Street, Cambridge, MA 02138, USA
[20] Laboratory for Multiwavelength Astrophysics, School of Physics and Astronomy, Rochester Institute of Technology, 84 Lomb Memorial Drive, Rochester, NY 14623, USA
[21] Center for Computational Astrophysics, Flatiron Institute, 162 Fifth Avenue, New York, NY 10010, USA
[22] Institute of Physics, GalSpec, Ecole Polytechnique Federale de Lausanne, Observatoire de Sauverny, Chemin Pegasi 51, 1290 Versoix, Switzerland
[23] INAF, Astronomical Observatory of Trieste, Via Tiepolo 11, I-34131 Trieste, Italy
[24] Max Planck Institute for Astronomy, Königstuhl 17, D-69117 Heidelberg, Germany
[25] Kapteyn Astronomical Institute, University of Groningen, P.O. Box 800, 9700 AV Groningen, The Netherlands
[26] Department of Astronomy, University of Massachusetts Amherst, MA 01003, USA
[27] Department of Physics, University of California, Santa Barbara, Santa Barbara, CA 93109, USA
[28] Kavli Institute for Astronomy and Astrophysics, Peking University, Beijing 100871, People's Republic of China
[29] Department of Astronomy and Astrophysics, University of California, Santa Cruz, 1156 High Street, Santa Cruz, CA 95064, USA
[30] Cosmic Dawn Center (DAWN), Copenhagen, Denmark
[31] Niels Bohr Institute, University of Copenhagen, Jagtvej 128, DK-2200, Copenhagen, Denmark
[32] Kavli Institute for the Physics and Mathematics of the Universe (WPI), The University of Tokyo, Kashiwa, Chiba 277-8583, Japan
[33] Department of Astronomy, School of Science, The University of Tokyo, 7-3-1 Hongo, Bunkyo, Tokyo 113-0033, Japan
[34] School of Physics and Astronomy, Tel Aviv University, Tel Aviv 69978, Israel
[35] Thüringer Landessternwarte, Sternwarte 5, D-07778 Tautenburg, Germany
[36] National Astronomical Observatory of Japan, 2-21-1 Osawa, Mitaka, Tokyo 181-8588, Japan
[37] Aix Marseille Univ, CNRS, CNES, LAM, Marseille, France
[38] Institut d'Astrophysique de Paris, UMR 7095, CNRS, and Sorbonne Université, 98 bis boulevard Arago, F-75014 Paris, France
[39] Jet Propulsion Laboratory, California Institute of Technology, 4800 Oak Grove Drive, Pasadena, CA 91001, USA
Received 2023 August 23; revised 2023 October 26; accepted 2023 November 17; published 2024 January 18

[40] NPP Fellow.
[41] NASA Hubble Fellow.
[42] NSF Graduate Research Fellow.
[43] Marie Curie Fellow.

Abstract

In this Letter, we report the discovery of the highest redshift, heavily obscured, radio-loud (RL) active galactic nucleus (AGN) candidate selected using JWST NIRCam/MIRI, mid-IR, submillimeter, and radio imaging in the COSMOS-Web field. Using multifrequency radio observations and mid-IR photometry, we identify a powerful, RL, growing supermassive black hole with significant spectral steepening of the radio spectral energy distribution ($f_{1.28\ \mathrm{GHz}} \sim 2$ mJy, $q_{24\ \mu\mathrm{m}} = -1.1$, $\alpha_{1.28-3\ \mathrm{GHz}} = -1.2$, $\Delta\alpha = -0.4$). In conjunction with ALMA, deep ground-based observations, ancillary space-based data, and the unprecedented resolution and sensitivity of JWST, we find no evidence of AGN contribution to the UV/optical/near-infrared (NIR) data and thus infer heavy amounts of obscuration ($N_{\mathrm{H}} > 10^{23}$ cm^{-2}). Using the wealth of deep UV to submillimeter photometric data, we report a singular solution photo-z of $z_{\mathrm{phot}} = 7.7^{+0.4}_{-0.3}$ and estimate an extremely massive host galaxy ($\log M_{\star} = 11.92 \pm 0.5 M_{\odot}$) hosting a powerful, growing supermassive black hole ($L_{\mathrm{Bol}} = 4-12\mathrm{x} \times 10^{46}$ erg s^{-1}). This source represents the farthest known obscured RL AGN candidate, and its level of obscuration aligns with the most representative but observationally scarce population of AGN at these epochs.

Unified Astronomy Thesaurus concepts: Quasars (1319); Radio loud quasars (1349); Active galactic nuclei (16); Supermassive black holes (1663); Reionization (1383); High-redshift galaxies (734)

1. Introduction

Recent discoveries of $z > 6$ extremely powerful ($L_{\mathrm{Bol}} \sim 10^{46}$ erg s^{-1}) active galactic nuclei (hereinafter referred to as AGN) have launched intense debate as to how such massive black holes ($\sim 10^{9} M_{\odot}$) can form so early in the Universe (Mortlock et al. 2011; Bañados et al. 2018; Inayoshi et al. 2020; Wang et al. 2021). Questions surrounding the triggering and growth of these AGN have largely remained unanswered. This is driven by the fact that almost all direct observations of $z > 6$ AGN are *unobscured*—the very energy that makes these sources detectable at high redshifts overwhelms the star-forming (SF) contributions from their host galaxies in rest-frame UV–near-infrared (NIR) imaging.

Thus it is paramount to observe powerful AGN at $z > 6$ whose central engines are heavily obscured for the following reasons: (1) Unlike with unobscured AGN, the host-galaxy properties of obscured AGN (e.g., $M_{\star}$, morphology) are more accessible in regimes where the AGN emission is significantly attenuated (i.e., rest-frame UV/optical). (2) According to a combination of theory and observations, over 80% of AGN are expected to be heavily obscured ($N_{\mathrm{H}} > 10^{23}$ cm^{-2}) by their host galaxies at $z > 6$ and over 99% by $z > 7$ (Ni et al. 2020; Gilli et al. 2022). The obscuration of AGN can occur over a vast range of physical scales and conditions. In the local Universe, obscured AGN are contextualized by the standard sight line–dependent unification scheme—where the dominant source of obscuration is thought to occur a few parsecs from the accretion disk by an optically thick toroidal or cloud structure and exhibit a lack of intrinsic difference between the host galaxy and black hole (BH) properties of their unobscured AGN counterparts (Antonucci 1993; Urry & Padovani 1995). New evidence is accumulating that at higher redshifts, the dominant sources of AGN obscuration may exist on kiloparsec scales (Circosta et al. 2019; D'Amato et al. 2020). In both theory and observations, it is shown that at increasing redshifts, galaxies are clumpy and less settled (Faure et al. 2021; Kartaltepe et al. 2023) and have higher inter-stellar medium (ISM) densities (Buchner et al. 2017; Dalton et al. 2021; Gilli et al. 2022). Therefore, it is unsurprising that recent studies find high AGN-obscured fractions due to the increased chances of UV/optical photons from the accretion disk being significantly attenuated along its path through its host galaxy (Ni et al. 2020; Gilli et al. 2022).

Recent JWST spectroscopic and photometric observations have yielded a litany of $z > 5$ actively accreting supermassive black holes (SMBHs; Furtak et al. 2023; Kocevski et al. 2023; Labbe et al. 2023; Larson et al. 2023; Maiolino et al. 2023; Matthee et al. 2023), yet for these sources—some of which are heavily reddened—their rest-frame UV-optical emission probes their AGN nature and thus by definition are not heavily obscured. Even JWST/MIRI spectra of $z \sim 7$ AGN probe rest-frame $\lesssim 2\ \mu$m emission (i.e., Bosman et al. 2023), and for the most obscured AGN, their nature may only be robustly revealed at rest-mid-infrared (MIR) wavelengths in lieu of sufficient detection of high-ionization lines (Hickox & Alexander 2018). Thus, these newly measured JWST sources may not represent the most common type of AGN at these epochs, and it is yet to be determined whether their formation and/or evolution is intrinsically different from the high-z obscured AGN population. From black hole seeds to AGN feedback, the interpretation of JWST-discovered high-z AGN candidates may be significantly impacted if there are different triggering pathways or host-galaxy properties of obscured versus unobscured AGN.

Despite the predicted increased number density of high-z heavily obscured AGN, their identification is incredibly difficult due to their heavy obscuration at wavelengths shorter than the MIR and lack of observing facilities that are capable of probing the rest-frame MIR at these epochs. Rest-frame optical-NIR spectroscopy will lack the characteristic broad lines evident in unobscured sources and requires careful analysis of multiple, well-detected narrow lines to constrain whether the source of the ionizing photons is dominated by AGN versus star-forming processes (Onoue et al. 2021). In addition, X-ray facilities are generally incapable of reaching the sensitivities required for other than a handful of sources at $z = 6$–7 (Vito et al. 2019) and a potentially lensed $z = 10$ source (Bogdán et al. 2023; Goulding et al. 2023). On the other hand, radio emissions can penetrate through dense columns of gas and dust, and current facilities can reach the required sensitivities. Still, AGN that exhibit a significant excess of *nonthermal* radio emission above what would be expected from star formation and thermal AGN contribution alone (defined as radio loud, RL) are rare (<10% of the total AGN population, Kellermann et al. 1989; Herrera Ruiz et al. 2017).

Interestingly, a powerful, heavily obscured radio source ($L_{\mathrm{Bol}} \sim 10^{46}$ erg s^{-1}) was discovered at $z \sim 7$ (COS-87259; Endsley et al. 2023)—and even this object posed more

questions than it answered. COS-87259, first identified in the COSMOS field thanks to the broad bandwidth and depths accessed in the COSMOS survey, was recently spectroscopically confirmed at $z = 6.8$ via [C II] detection in Atacama Large Millimeter/submillimeter Array (ALMA) Band 6 observations (Endsley et al. 2023). Bona fide evidence of the central engine in COS-87259 was discovered due to its bright radio emission. At $z \sim 7$, space density estimates of UV-bright sources are estimated to be $1/3000\,\mathrm{deg}^2$ (Shen et al. 2020), and for powerful RL AGN, $1/5000\,\mathrm{deg}^2$ (Ighina et al. 2023)—yet this source was found in an Hyper-Suprime Cam $1.5\,\mathrm{deg}^2$ survey.

Current UV-based, absorption-corrected space density estimates imply that 10% of the cosmic black hole growth in the Universe occurred by $z = 6$ with a rapid buildup of growth occurring between $z = 4$ and 2 (Shen et al. 2020; Matsuoka et al. 2023). Increasing the number density of obscured sources above $z = 6$ inspires several nuanced questions: Is there a significant reshaping of the gas distribution in AGN host galaxies that rapidly occurs between $z = 7$ and 6? Are the UV-bright AGN a much smaller tail of a larger AGN population—and thus, our understanding of the number density estimates and accretion history of SMBHs over cosmic time needs to be overhauled? It is difficult to answer these questions when only one heavily obscured AGN at $z \sim 7$ has been identified, i.e., COS-87259.

In this Letter, we report the discovery of COSW-106725 in the COSMOS-Web field. This source was initially detected in the NIR (UVISTA + Hubble Space Telescope, HST, WFC3IR), radio (Very Large Array, VLA + Very Long Baseline Array, VLBA), and submillimeter (ALMA 343 GHz continuum). During the 2023 April JWST Cycle 1 COSMOS-Web program observations, four NIRCam + one MIRI bands were imaged. Section 2 describes the observations of X-ray to submillimeter data of the source. Section 3 reports the results from spectral energy distribution (SED) fitting and describes the derived AGN and galaxy properties. Section 4 compares the source to the only similar source on record and contextualizes these findings regarding high-z obscured AGN demographics. In Section 4, we present the summary and conclusion. We use an $h = 0.7$, $\Omega_m = 0.3$, $\Omega_\Lambda = 0.7$ cosmology throughout this paper.

2. Multiwavelength Observations of COSW-106725

The target was first erroneously classified over 10 yr ago during a search for low-luminosity radio galaxies at cosmic noon within the COSMOS field (COSMOS-FRI-07; see Chiaberge et al. 2009 for details). COSMOS is a deep, wide-area, multiwavelength survey centered on R.A. 10:00:30.12, decl. +2:12:38.80 (Scoville et al. 2007). Extensive observations of the field from almost all major space- and ground-based telescopes have accrued over the past 20 yr (Laigle et al. 2016; Weaver et al. 2022). The initial basic selection criteria of Chiaberge et al. (2009) were based on the initial COSMOS multiwavelength catalog (Capak et al. 2007) and initial VLA 1.4 GHz observations (Bondi et al. 2008). This required the radio flux (at 1.4 GHz) to be between 1 and 13 mJy and the optical magnitude to be higher than $i+ = 21$ (Vega). Although COSW-106725 made the initial sample selection in the radio range, the source was erroneously associated with the combined optical detections of a bright star and a lower-z interloper within $2''$ of the radio coordinates. The initial NIR (CFHT) and MIR (Spitzer/IRAC; Sanders et al. 2007) fluxes were also highly uncertain due to poor spatial resolution and multiple interlopers. The limiting spatial resolution of the optical-MIR data and the disconcordance between the radio and the source's optical properties were noted, and the nature of the object was left unknown.

In the past 10 yr, deeper imaging and new wavelength coverage have been taken in the COSMOS field. In addition to deeper radio data, larger radio coverage and a growing number of ALMA observations—the central $0.54\,\mathrm{deg}^2$ of the COSMOS field—were chosen for the largest JWST program scheduled for observations during the observatory's first cycle in both sky coverage and total prime-time allocation (COSMOS-Web Survey, PID #1727; PIs: Kartaltepe & Casey; Casey et al. 2022). COSMOS-Web consists of one large contiguous $0.54\,\mathrm{deg}^2$ NIRCam mosaic conducted in four filters, with additional MIRI imaging covering $0.18\,\mathrm{deg}^2$, and will be completed by 2024 January. Within the current $0.27\,\mathrm{deg}^2$ covered, this combination of new data in the COSMOS field has lifted the veil of uncertainty around COSW-106725 and allowed us to identify the highest-redshift heavily obscured RL AGN candidate to date. In the following subsections, we highlight the relevant observations conducted since the initial discovery of COSW-106725.

2.1. Radio

The COSMOS field has been observed over a large range of radio wavelengths (144 MHz–3 GHz) via the VLA, VLBA, the Giant Metrewave Radio Telescope (GMRT), and the international Low-Frequency Array. COSW-106725 was strongly detected with GMRT 324 MHz (6.27 ± 0.480 mJy) and VLA 324 MHz (6.93 ± 0.5 mJy; Smolčić et al. 2014), MeerKAT 1.28 GHz ($1.99 \pm 8.8 \times 10^{-3}$ mJy; Hale et al. 2023), VLA 1.4 GHz (1.78 ± 0.15 mJy; Bondi et al. 2008), VLBA + GBT 1.4 GHz (1.84 ± 0.1 mJy; Herrera Ruiz et al. 2017), and VLA 3 GHz (0.776 ± 0.04 mJy; Smolčić et al. 2017). The physical extent of the VLA 3 GHz detection deconvolved with the beam is $<2\farcs2$.

COSW-106725 is also detected as a compact source at the $\sim 5\sigma$ level in all three epochs of the VLA Sky Survey (VLASS; Lacy et al. 2020). The peak flux density averaged over the three VLASS epochs and measured from the quick-look image products is $0.711\,\mathrm{mJy\,beam}^{-1}$. This measurement is consistent with the VLA 3 GHz measurement reported in Table 1. We do not find any evidence for significant variability at 3 GHz given the typical 20% flux scale uncertainty in VLASS quick-look data. To our knowledge, COSW-106725 is the highest-redshift source detected in VLASS so far, surpassing the VLASS detection of a quasar at $z \sim 6.2$ in Bañados et al. (2023). Furthermore, there is a robust detection of COSW-106725 from the VLA Low-Band Ionosphere and Transient Experiment (VLITE),[44] which commensally records data at a center frequency of 338 MHz with nearly all VLA observations (Clarke et al. 2018; Polisensky et al. 2019). COSW-106725 was detected across many individual observations with VLITE. The average total flux of the source is 6.63 ± 1.05 mJy taking into account the 15% flux uncertainties of VLITE.

In Figure 1, we plot the radio SED of COSW-106725. Using $S_\nu \propto \nu^\alpha$, we measure the radio slope between 144 MHz and 1.28 GHz ($\alpha_{.144-1.28} = -0.82$) and the radio slope between

[44] https://vlite.nrao.edu

Table 1
Multiwavelength Ground- and Space-based Photometry for COSW-106725

Band	Flux (μJy)
Subaru/HSC g	<0.021
Subaru/HSC r	<0.034
Subaru/HSC i	<0.043
HST/WFC3 F814W	<0.048
Subaru/HSC z	<0.063
Subaru/HSC y	<0.093
JWST/NIRCam F115W	0.092 ± 0.002
JWST/NIRCam F150W	0.21 ± 0.009
HST/WFC3 F160W	0.22 ± 0.011
JWST/NIRCam F277W	1.0 ± 0.09
Spitzer/IRAC 3.6 μm	3.05 ± 0.4
JWST/NIRCam F444W	5.34 ± 0.05
Spitzer/IRAC 4.5 μm	5.5 ± 0.49
Spitzer/IRAC 5.8 μm	7.71 ± 0.57
JWST/MIRI F770W	11.0 ± 1.33
Spitzer/MIPS 24 μm	91.3 ± 27.2
Herschel/PACS 100 μm	0.0012
Herschel/PACS 160 μm	0.0053
Herschel/SPIRE 250 μm	0.021
Herschel/SPIRE 350 μm	0.023
Herschel/SPIRE 500 μm	0.012
JCMT/SCUBA-2 850 μm	0.026
ALMA 343 GHz	$2.5 \times 10^3 \pm 5 \times 10^4$
VLA 3 GHz	$0.776 \times 10^3 \pm 0.04 \times 10^4$
VLA 1.4 GHz	$1.78 \times 10^3 \pm 0.15 \times 10^4$
MeerKAT 1.28 GHz	$1.99 \times 10^3 \pm 8.8$
GMRT 610 MHz	$3.43 \times 10^3 \pm 1.7 \times 10^4$
VLITE 338 MHz	$6.63 \times 10^3 \pm 1.1 \times 10^3$
VLA 324 MHz	$6.92 \times 10^3 \pm 4.8 \times 10^4$
GMRT 324 MHz	$6.27 \times 10^3 \pm 3.1 \times 10^4$

Note. All upper limits are at the 3σ level.

1.32 and 3 GHz ($\alpha_{1.28-3} = -1.1$). This spectral steepening toward higher frequencies is consistent not only with the reported radio properties of COS-87259 but also with the behavior of many spectroscopically confirmed $z > 4$ RL AGN (Miley & De Breuck 2008; Saxena et al. 2018b; Drouart et al. 2020; Yamashita et al. 2020; Broderick et al. 2022).

Finally, we compare the Spitzer MIPS 24 μm and VLA 1.4 GHz fluxes to assess the level of nonthermal AGN contribution to the radio emission. The observed 24 μm and 1.4 GHz fluxes are tightly related for thermal sources (i.e., non-RL AGN and star-forming galaxies). Using the parameterization in Bonzini et al. (2013), we measure the value of $q_{24\mathrm{obs}} = \log_{10}(f_{24\,\mu\mathrm{m}}/f_{1.4\,\mathrm{GHz}}) = -1.1$, indicating the presence of powerful radio emission due to a kiloparsec-scale jetted AGN or compact radio source versus thermal emission associated with radio-quiet AGN and/or star formation.

2.2. ALMA

COSW-106725 has a robust 5σ detection ($F_{\mathrm{int}} = 2.5 \pm 0.5$ mJy) in $\sim$870 μm band continuum imaging via the A3COSMOS catalog (Liu et al. 2019). The A3COSMOS catalog used the rich public ALMA archive to generate automated mining pipelines across the COSMOS field. We use the Gaussian fit flux via the "blind" pipeline. We note the "prior"-fitting photometry catalog yields an equivalent flux measurement (see Liu et al. 2019 for details).

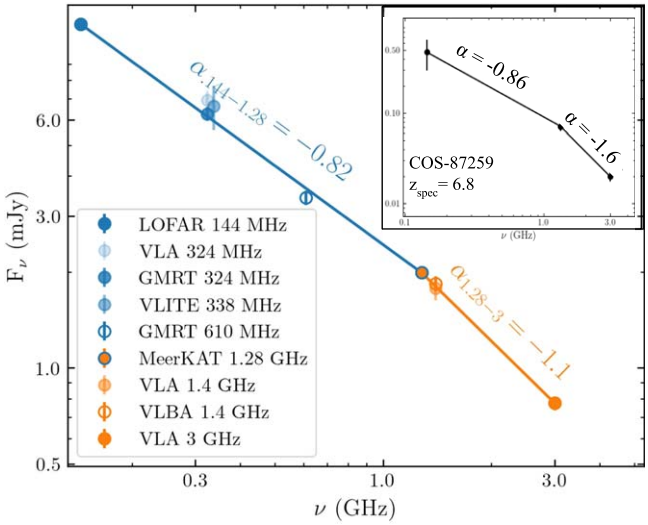

Figure 1. Radio SED: all fluxes and associated errors are listed in Table 1. We measure the spectral slope between two sets of radio frequencies (blue line, orange line) and find significant spectral steepening indicative of high-z RL AGN (Saxena et al. 2018a; Broderick et al. 2022; Endsley et al. 2023). In the upper-right corner inset, we show the radio SED for the $z_{\mathrm{spec}} = 6.8$ heavily obscured RL AGN from Endsley et al. (2023) for reference.

2.3. X-Ray

The source was previously covered with the Chandra ACIS-I detector (160 ks; Civano et al. 2016) and the XMM-Newton PN, MOS1, and MOS2 detections (30 ks; Cappelluti et al. 2009). This source is undetected in the Chandra-Legacy survey of the COSMOS field and the XMM-COSMOS survey (Cappelluti et al. 2009; Civano et al. 2016). We calculate the upper limit 2–10 keV flux in the 160 ks combined event image using the `CIAO` tools function `aprates` (Fruscione et al. 2006) and find $F_{2-10\,\mathrm{keV}} < 2.3 \times 10^{-15}$ erg s^{-1} cm^{-2}. In Section 4, we further discuss the X-ray upper limits.

2.4. Additional Ground- and Space-based Optical/NIR/MIR Imaging

All optical upper limits are drawn from the "classic" COSMOS2020 catalog (Weaver et al. 2022). Included in COSMOS2020 is ultra-deep, broadband photometry from the second public data release of the Hyper Suprime-Cam (HSC) Subaru Strategic Program comprising the g, r, i, z, and y bands. COSW-106725 is undetected in all bands (g: $\mathrm{mag_{lim}} = 28.1$, r: $\mathrm{mag_{lim}} = 27.8$, i: $\mathrm{mag_{lim}} = 27.6$, z: $\mathrm{mag_{lim}} = 27.2$, and y: $\mathrm{mag_{lim}} = 26.5$). HST/ACS F814W high-resolution photometry is also included, and the object remains undetected ($\mathrm{mag_{lim}} = 27.8$).

A search of COSW-106725's radio coordinates in MAST serendipitously finds a WFC3IR F160W image of another source covered in an unrelated HST campaign (PI: Conselice, Cycle 24, GO:14721). Using Source Extractor (SE; Bertin & Arnouts 1996) on the MAST reduced image, we measure a 1″ aperture F160W flux that agrees with the JWST F150W flux. This source is also detected in all four Spitzer IRAC bands and MIPS 24 μm. We use the source locations in the JWST NIRCam F277W and radio bands to de-blend the Spitzer photometry and find excellent photometric agreement with JWST NIRCam F444W and IRAC Ch 2 (see Jin et al. 2018 for details).

The positional accuracy of the radio, ALMA, and JWST emission are all within 1″. All fluxes and upper limits are listed in Table 1.

2.5. JWST NIRCam+MIRI Imaging

This object is in the Cycle 1 JWST COSMOS-Web field (GO #1727, PIs: Kartaltepe & Casey; Casey et al. 2022), with observations available in four NIRCam wide-band filters: F115W, F150W, F277W, and F444W, and one MIRI wide-band filter: F770W. Forthcoming papers will comprehensively describe the complete data reduction process (COSMOS-Web NIRCam; M. Franco et al. 2024, in preparation, COSMOS-Web MIRI; S. Harish et al. 2024, in preparation), but we briefly outline the procedures here. Upon retrieval of the uncalibrated NIRCam images from the STScI MAST Archive, we reduced the data utilizing the JWST Calibration Pipeline (Bushouse et al. 2022). Custom modifications were incorporated, such as mitigating $1/f$ noise and subtracting low-level background, following the precedent set by other JWST studies (e.g., Bagley et al. 2023). All reference files, including in-flight data, represented the latest calibrations available during our observations. The final mosaics were generated during Stage 3 of the pipeline, varying only in resolution, with pixel sizes of 0.″03 pixel^{-1} and 0.″06 pixel^{-1}. Unless otherwise specified, we will refer to the 0.″06 pixel^{-1} resolution mosaic hereafter. The JWST mosaics were aligned to a version of the COSMOS F814W mosaic (Koekemoer et al. 2007) that had been astrometrically aligned to Gaia DR3, with the F814W mosaic subsequently used as a reference catalog for all the JWST imaging (Koekemoer et al. 2007). The median offset between the F814W mosaic and the COSMOS-Web NIRCam mosaic is less than 5 mas.

The MIRI F770W observations were also reduced using the JWST Calibration pipeline and with the additional background subtraction step to mitigate instrumental effects. The F770W mosaic was then resampled to an output grid corresponding to 0.″06 pixel^{-1} and aligned with the HST ACS F814W imaging. We perform source detection and measure the multiwavelength aperture photometry of the COSMOS-Web data using SE V 2.86 (Bertin & Arnouts 1996). We use 1″ apertures and apply a detection threshold corresponding to a signal-to-noise ratio of 3. In Figure 2, we show a selection of postage stamp images of COSW-10675.

3. Results

3.1. Photo-z Estimate via Optical/NIR/MIR Photometry

With the photometry listed in Table 1, we first run EAzY, a template-based SED fitting code (Brammer et al. 2008). EAzY generates a photo-z probability density function via χ^2 minimization using linear combinations of predefined templates. We use the standard 12 template FSPS set included in EAzY (tweak_fsps_QSF_12_v3) and the six additional templates from Larson et al. (2023). In conjunction with the deep ground-based data and the unprecedented resolution and sensitivity of JWST—we perform robust SED fitting on the source and find a singular solution photo-z estimate of $z_{\rm phot} = 7.7^{+0.4}_{-0.3}$ with reduced $\chi^2 = 0.3$.

The Balmer break spectral region is well sampled with IRAC +JWST observations, and the Lyman break is sampled via deep HSC/HST+JWST observations. The detection level in F115W places a strict $z < 8$ constraint. In Figure 3, we also show (gray lines) the fits to templates of heavily dust-obscured star-forming galaxies at $z < 7$. The HST F160W + JWST F150W/F277W detections heavily disfavor any templates with $2 < z < 7$, while the MIRI F770W detection solidly rules out the $z \geqslant 2$ templates. The IRAC data used in the fit well samples the data as is evidenced by the similar fluxes in IRAC Ch 2 (4.5 μm) and JWST F444W (4.4 μm). In addition to the fit photo-z, the ancillary observations of this source robustly constrain the redshift to within $z = 7$–8.

We also independently measure the photo-z using BAGPIPES using a delayed-tau star formation history ($\log(M_*/M_\odot) \sim 6$–13, $Z \sim 0.001$–2.5, $\tau \sim 0.1$–5 Gyr, Age $\sim$ 0%–100% $t_{\rm H}$), constant starburst (age $\sim$ 1–100 Myr), nebular emission ($\log U \sim -4$ to -1), flexible dust attenuation law ($A_V \sim 0$–3, slope allowed to vary with a Gaussian prior centered on an SMC dust law), and redshift ($z \sim 0$–12). We find a consistent photo-z ($z = 7.5 \pm 0.35$, $\chi^2 = 0.27$), $A_V \sim 2$, and a $M_* = 2.8$–$5.4 \times 10^{11}\ M_\odot$. In Figure 3, we overlay the BAGPIPES $p(z)$ in the lower-left inset.

3.2. SED Decomposition at Best-fit Photo-z

Using the photo-z derived via EAzY, we then fit the global optical-IR-radio SED with a composite of SED components accounting for stars, mid-IR AGN, dust, and radio emission to produce tighter constraints on the stellar mass and infer the AGN bolometric luminosity (Figure 4). We use the MICHI2 code[45] to fit multiple SED components simultaneously: (a) the Bruzual & Charlot (2003, hereafter BC03) synthesized stellar templates (with a constant star formation history and Calzetti et al. 2010 attenuation law), (b) the low-redshift observationally constructed mid-IR AGN templates (Mullaney et al. 2011), (c) the widely used Draine & Li dust models (Draine & Li 2007), and (d) a power-law radio component with a spectral index 0.8, consistent for most RL AGN (Smolčić et al. 2017).

The best-fit SED shows a strong contribution from the AGN in the mid-IR, dominating the 20–200 μm emission. The $1/\chi^2$ distributions representing the parameter probabilities are shown in the right panels of Figure 4. Taking into account the redshift posterior distribution in the error propagation from EAzY, we find a well-constrained stellar mass $\sim 10^{11.92\pm0.5}\,M_\odot$, dust attenuation of $E(B-V) \sim 0.68 \pm 0.08$, and a loosely constrained dust infrared luminosity $\sim 10^{12}\,L_\odot$ (which has the AGN contribution subtracted).

The fitted AGN luminosity integrated over 10–1000 μm is $\sim$1–3 $\times 10^{13}\,L_\odot$, corresponding to an AGN bolometric luminosity of $\sim$4–12 $\times 10^{46}$ erg s^{-1} via the bolometric correction provided in Delvecchio et al. (2014). The bolometric luminosity of the source, coupled with the lack of any point source in the NIR images and lack of detection in the Chandra-Legacy 160 ks survey, allows us to infer the level of obscuration of the AGN to be $N_{\rm H} > 10^{23}\,{\rm cm}^{-2}$. Given that this quasar is heavily obscured in the optical, we do not include a rest-frame UV-optical quasar template in our fitting.

Next, we compare the above SED-derived $L_{\rm Bol}$ to the $L_{\rm Bol}$ estimated from the X-ray upper limit. We apply the correction provided in Duras et al. (2020) to estimate the hard-band X-ray luminosity from the bolometric luminosity derived via SED fitting and calculate $L_{2-10\,{\rm keV,SED}} = 2$–$10 \times 10^{44}$ erg s^{-1}. We then calculate the X-ray 2–10 keV luminosity using the X-ray flux upper limit derived in Section 2.3 and the photo-z estimated from

[45] https://github.com/1054/Crab.Toolkit.michi2 (Liu et al. 2021).

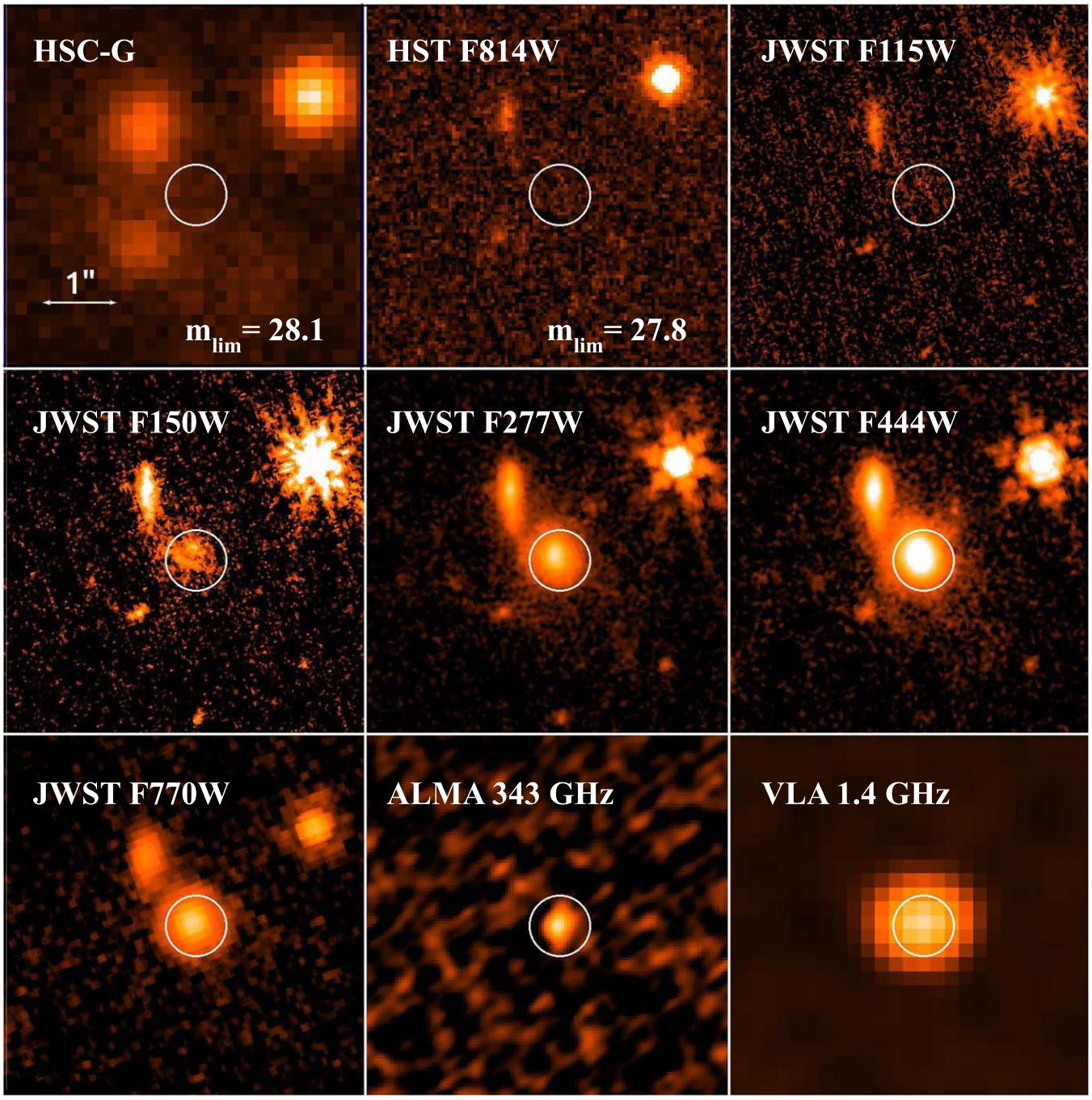

Figure 2. Selection of postage stamp images of the candidate $z \sim 7.7$ RL AGN, COSW-106725. Top row, from left to right: HSC-*g*, HST Advanced Camera for Surveys F814W, JWST F115W. Middle row: JWST F150W, JWST F277W, JWST F444W. Bottom row: JWST MIRI F770W, ALMA 343 GHz, and VLA 1.4 GHz. The ALMA extent is overlaid on each image (in white). The 3σ upper limits are reported for the non-detections. The upper left source in the UV/Optical/NIR images is a low-z interloper (Weaver et al. 2022).

Section 3.1 and find $L_{2-10\,\mathrm{keV,X-ray}} < 1.5 \times 10^{45}\,\mathrm{erg\,s^{-1}}$. Thus, assuming this object is at $z \sim 7.7$, the bolometric luminosity derived from the optical–submillimeter SED fit agrees with the X-ray-based upper limit estimate.

4. Discussion and Conclusions

Assuming Eddington accretion, $\lambda_{\mathrm{Edd}} = 1$, we provide a lower limit to the BH mass of COSW-106725. Following the canonical Eddington luminosity relationship using $L_{\mathrm{Bol}} = 5.1 \times 10^{46}\,\mathrm{erg\,s^{-1}}$, we find $M_{\mathrm{BH}} \geqslant 6.4 \times 10^{8}\,M_{\odot}$. While this number is only a lower limit, we can calculate whether COSW-106725 is potentially more massive than expected by comparing the M_* derived from the SED fit in Section 3.2 to the M_* derived from local M_{BH} versus M_* scaling relations. Using Equation (8) from Ding et al. (2020), we find that the comparable stellar mass for this black hole mass should be M_*=3.69 $\times 10^{11}\,M_{\odot}$. Due to the M_{BH} being a lower limit, the scaling-relation derived M_* is also a lower limit and is below the SED fit–derived M_* value (8.3 $\times 10^{11}\,M_{\odot}$). Thus, our estimated M_{BH} does not indicate an over-massive BH concerning its host galaxy.

In summary, we report the discovery of COSW-106725 in the COSMOS-Web field. The coincident radio/submillimeter/JWST

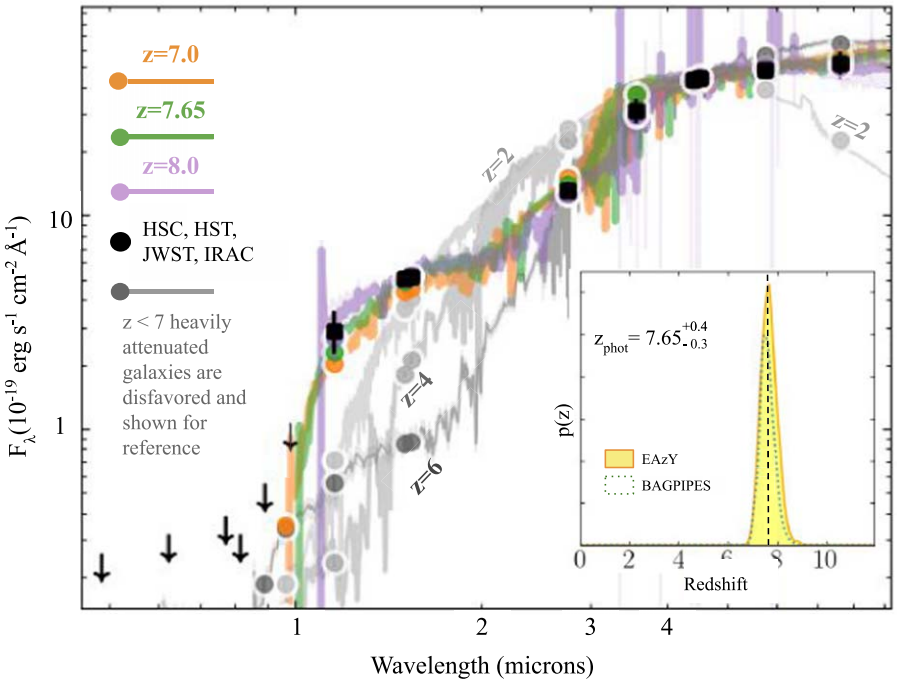

Figure 3. Results from fitting the optical, NIR, and MIR with *EAzYpy*. Non-detections with 27 mag upper limits: HSC g, HSC r, HSC i, HSC z, HST F814W, HSC y. $> 3\sigma$ detections: JWST F115W, JWST F150W, HST F160W, JWST F277W, IRAC Channel 1, JWST F444W, IRAC Channel 2, IRAC Channel 3, JWST MIRI 7.7 μm. The redshift is constrained to $z = 7.7^{+0.4}_{-0.3}$ fit with combinations of simple stellar population templates from Bruzual & Charlot (2003). Inset: we show the $p(z)$ via EAzY and BAGPIPES

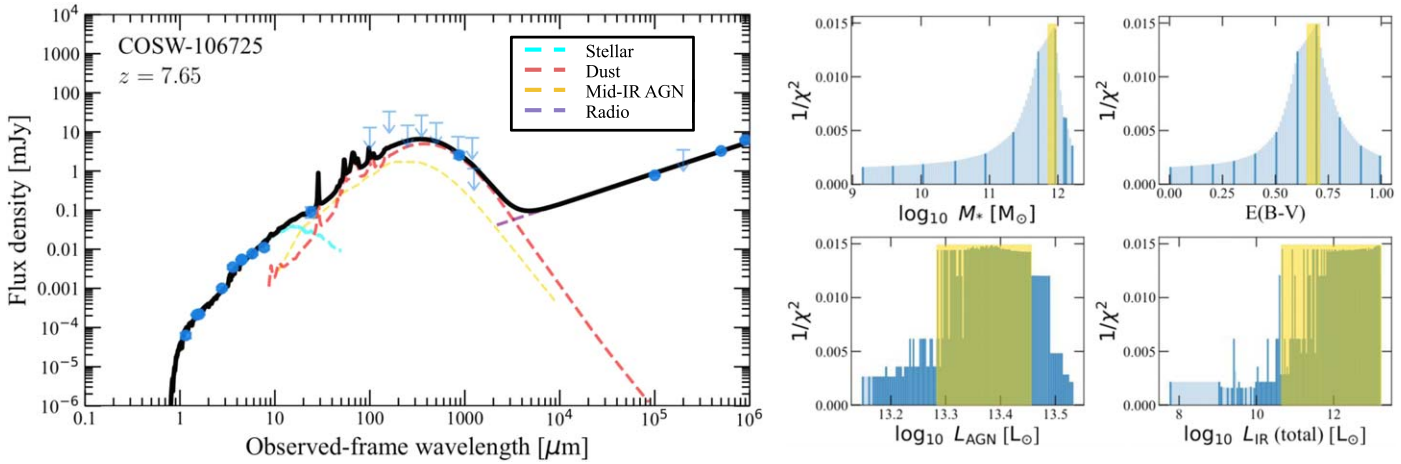

Figure 4. Left panel: optical-IR-radio SED fitting with BC03 stellar (Bruzual & Charlot 2003), mid-IR AGN (Mullaney et al. 2011), Draine & Li dust (Draine & Li 2007), and power-law radio templates (using the MICHI2 code; Liu et al. 2021). The black line indicates the composite best-fit model, and the blue symbols are photometric data points, with upper limits shown as downward arrows. The stellar, mid-IR AGN, dust, and radio components are indicated by the cyan, yellow, red, and magenta dashed lines, respectively. Right panels: the $1/\chi^2$ distributions from the fitting for the four parameters: stellar mass, dust attenuation $E(B-V)$, AGN component's luminosity integrated over 10–1000 μm, and dust component's luminosity integrated over 8–1000 μm. The yellow highlighted regions correspond to the 95% confidence intervals.

observations of the source provide a robust estimate of $z_{\rm phot} = 7.7$. This source is first detected in the rest-frame optical via JWST F115W and remains undetected in deep space- and ground-based 0.4–1 μm imaging. Due to the high-inferred $L_{\rm Bol} = 5.1 \times 10^{46}$ erg s^{-1} and lack of significant AGN emission in the rest-frame optical/NIR/X-ray, the source is inferred to be an intrinsically powerful and heavily obscured ($N_{\rm H} > 10^{23}$ cm^{-2}) AGN, thus leading to its classification as a type 2 AGN candidate. The detection of this source (COSW-106725) and COS-87259 (Endsley et al. 2023) within the epoch of $z = 6.8$–8 in a 1.5 deg^2 field hints that the space density of luminous, RL AGN at these epochs may be underestimated by over a factor of 2000. Even in the local Universe, RL AGN are only a subset of the total AGN population (<10%) and at $z = 7$ up to now have had a measured space density of 1/5000 deg^2 (Ighina et al. 2023). Thus, the discovery of two RL, heavily obscured AGN within 1.5 deg^2 at $z \sim 7$ is at the intersection of increasing improbability (Ighina et al. 2023).

For there to be more AGN in the Epoch of Reionization than predicted via extrapolation of luminosity functions at lower redshifts, a very rapid change in the gas properties of AGN host galaxies must occur (Vito et al. 2018). Selecting heavily

obscured sources at high redshift remains challenging even with JWST, and answering the nuanced questions surrounding early BH formation and growth with sparse data sets is challenging. Thus, combining JWST imaging with deep radio data can potentially revolutionize our understanding of powerful, obscured sources at cosmic dawn by enabling their efficient selection.

Acknowledgments

We thank the anonymous referees for their thoughtful insight and important contributions to this work. E.L.L. and T.A.H. are supported by appointment to the NASA Postdoctoral Program (NPP) at NASA Goddard Space Flight Center, administered by Oak Ridge Associated Universities under contract with NASA. The National Radio Astronomy Observatory is a facility of the National Science Foundation operated under cooperative agreement by Associated Universities, Inc. Basic research in radio astronomy at the U. S. Naval Research Laboratory is supported by 6.1 Base funding. Construction and installation of VLITE was supported by the NRL Sustainment Restoration and Maintenance fund. ALMA is a partnership of ESO (representing its member states), NSF (USA) and NINS (Japan), together with NRC (Canada), MOST and ASIAA (Taiwan), and KASI (Republic of Korea), in cooperation with the Republic of Chile. The Joint ALMA Observatory is operated by ESO, AUI/NRAO and NAOJ. Support for this work was provided by NASA through grant JWST-GO-01727 and HST-AR-15802 awarded by the Space Telescope Science Institute, which is operated by the Association of Universities for Research in Astronomy, Inc., under NASA contract NAS 5-26555. Some of the data presented in this paper were obtained from the Mikulski Archive for Space Telescopes (MAST) at the Space Telescope Science Institute. The specific observations analyzed can be accessed via doi:10.17909/ym93-d513.

Software: pandas (McKinney 2010), scipy (Virtanen et al. 2020), ipython (Pérez & Granger 2007), matplotlib (Hunter 2007), BAGPIPES (Carnall et al. 2019), astropy (Astropy Collaboration et al. 2013), EAzY (Brammer et al. 2008).

ORCID iDs

Erini Lambrides https://orcid.org/0000-0003-3216-7190
Marco Chiaberge https://orcid.org/0000-0003-1564-3802
Arianna S. Long https://orcid.org/0000-0002-7530-8857
Daizhong Liu https://orcid.org/0000-0001-9773-7479
Hollis B. Akins https://orcid.org/0000-0003-3596-8794
Andrew F. Ptak https://orcid.org/0000-0001-5655-1440
Irham Taufik Andika https://orcid.org/0000-0001-6102-9526
Alessandro Capetti https://orcid.org/0000-0003-3684-4275
Caitlin M. Casey https://orcid.org/0000-0002-0930-6466
Jaclyn B. Champagne https://orcid.org/0000-0002-6184-9097
Katherine Chworowsky https://orcid.org/0000-0003-4922-0613
Tracy E. Clarke https://orcid.org/0000-0001-6812-7938
Olivia R. Cooper https://orcid.org/0000-0003-3881-1397
Xuheng Ding https://orcid.org/0000-0001-8917-2148
Dillon Z. Dong https://orcid.org/0000-0001-9584-2531
Andreas L. Faisst https://orcid.org/0000-0002-9382-9832
Jordan Y. Forman https://orcid.org/0000-0002-2077-2046
Maximilien Franco https://orcid.org/0000-0002-3560-8599
Steven Gillman https://orcid.org/0000-0001-9885-4589
Ghassem Gozaliasl https://orcid.org/0000-0002-0236-919X
Kirsten R. Hall https://orcid.org/0000-0002-4176-845X
Santosh Harish https://orcid.org/0000-0003-0129-2079
Christopher C. Hayward https://orcid.org/0000-0003-4073-3236
Michaela Hirschmann https://orcid.org/0000-0002-3301-3321
Taylor A. Hutchison https://orcid.org/0000-0001-6251-4988
Knud Jahnke https://orcid.org/0000-0003-3804-2137
Shuowen Jin https://orcid.org/0000-0002-8412-7951
Jeyhan S. Kartaltepe https://orcid.org/0000-0001-9187-3605
Emma T. Kleiner https://orcid.org/0009-0008-4614-5818
Anton M. Koekemoer https://orcid.org/0000-0002-6610-2048
Vasily Kokorev https://orcid.org/0000-0002-5588-9156
Sinclaire M. Manning https://orcid.org/0000-0003-0415-0121
Crystal L. Martin https://orcid.org/0000-0001-9189-7818
Jed McKinney https://orcid.org/0000-0002-6149-8178
Colin Norman https://orcid.org/0000-0002-5222-5717
Kristina Nyland https://orcid.org/0000-0003-1991-370X
Masafusa Onoue https://orcid.org/0000-0003-2984-6803
Brant E. Robertson https://orcid.org/0000-0002-4271-0364
Marko Shuntov https://orcid.org/0000-0002-7087-0701
John D. Silverman https://orcid.org/0000-0002-0000-6977
Massimo Stiavelli https://orcid.org/0000-0001-9935-6047
Benny Trakhtenbrot https://orcid.org/0000-0002-3683-7297
Eleni Vardoulaki https://orcid.org/0000-0002-4437-1773
Jorge A. Zavala https://orcid.org/0000-0002-7051-1100
Natalie Allen https://orcid.org/0000-0001-9610-7950
Olivier Ilbert https://orcid.org/0000-0002-7303-4397
Henry Joy McCracken https://orcid.org/0000-0002-9489-7765
Louise Paquereau https://orcid.org/0000-0003-2397-0360
Jason Rhodes https://orcid.org/0000-0002-4485-8549
Sune Toft https://orcid.org/0000-0003-3631-7176

References

Antonucci, R. 1993, ARA&A, 31, 473
Astropy Collaboration, Robitaille, T. P., Tollerud, E. J., et al. 2013, A&A, 558, A33
Bagley, M. B., Finkelstein, S. L., Koekemoer, A. M., et al. 2023, ApJL, 946, L12
Bañados, E., Schindler, J.-T., Venemans, B. P., et al. 2023, ApJS, 265, 29
Bañados, E., Venemans, B. P., Mazzucchelli, C., et al. 2018, Natur, 553, 473
Bertin, E., & Arnouts, S. 1996, A&AS, 117, 393
Bogdán, A., Goulding, A., Natarajan, P., et al. 2023, NatAs, Advanced Online Publication
Bondi, M., Ciliegi, P., Schinnerer, E., et al. 2008, ApJ, 681, 1129
Bonzini, M., Padovani, P., Mainieri, V., et al. 2013, MNRAS, 436, 3759
Bosman, S. E. I., Álvarez-Márquez, J., Colina, L., et al. 2023, arXiv:2307.14414
Brammer, G. B., van Dokkum, P. G., & Coppi, P. 2008, ApJ, 686, 1503
Broderick, J. W., Drouart, G., Seymour, N., et al. 2022, PASA, 39, e061
Bruzual, G., & Charlot, S. 2003, MNRAS, 344, 1000
Buchner, J., Schulze, S., & Bauer, F. E. 2017, MNRAS, 464, 4545
Bushouse, H., Eisenhamer, J., Dencheva, N., et al. 2022, JWST Calibration Pipeline, v1.8.2, Zenodo, doi:10.5281/zenodo.7325378
Calzetti, D., Wu, S. Y., Hong, S., et al. 2010, ApJ, 714, 1256
Capak, P., Aussel, H., Ajiki, M., et al. 2007, ApJS, 172, 99
Cappelluti, N., Brusa, M., Hasinger, G., et al. 2009, A&A, 497, 635

Carnall, A. C., Leja, J., Johnson, B. D., et al. 2019, ApJ, 873, 44
Casey, C. M., Kartaltepe, J. S., Drakos, N. E., et al. 2022, ApJ, 954, 31
Chiaberge, M., Tremblay, G., Capetti, A., et al. 2009, ApJ, 696, 1103
Circosta, C., Vignali, C., Gilli, R., et al. 2019, A&A, 623, A172
Civano, F., Marchesi, S., Comastri, A., et al. 2016, ApJ, 819, 62
Clarke, T., Peters, W., Brisken, W., et al. 2018, AAS Meeting Abstracts, 231, 354.11
Dalton, T., Morris, S. L., & Fumagalli, M. 2021, MNRAS, 502, 5981
D'Amato, Q., Gilli, R., Vignali, C., et al. 2020, A&A, 636, A37
Delvecchio, I., Gruppioni, C., Pozzi, F., et al. 2014, MNRAS, 439, 2736
Ding, X., Silverman, J., Treu, T., et al. 2020, ApJ, 888, 37
Draine, B. T., & Li, A. 2007, ApJ, 657, 810
Drouart, G., Seymour, N., Galvin, T. J., et al. 2020, PASA, 37, e026
Duras, F., Bongiorno, A., Ricci, F., et al. 2020, A&A, 636, A73
Endsley, R., Stark, D. P., Lyu, J., et al. 2023, MNRAS, 520, 4609
Faure, B., Bournaud, F., Fensch, J., et al. 2021, MNRAS, 502, 4641
Fruscione, A., McDowell, J. C., Allen, G. E., et al. 2006, Proc. SPIE, 6270, 62701V
Furtak, L. J., Labbé, I., Zitrin, A., et al. 2023, arXiv:2308.05735
Gilli, R., Norman, C., Calura, F., et al. 2022, A&A, 666, A17
Goulding, A. D., Greene, J. E., Setton, D. J., et al. 2023, ApJL, 955, L24
Hale, C. L., Whittam, I. H., Jarvis, M. J., et al. 2023, MNRAS, 520, 2668
Herrera Ruiz, N., Middelberg, E., Deller, A., et al. 2017, A&A, 607, A132
Hickox, R. C., & Alexander, D. M. 2018, ARA&A, 56, 625
Hunter, J. D. 2007, CSE, 9, 90
Ighina, L., Caccianiga, A., Moretti, A., et al. 2023, MNRAS, 519, 2060
Inayoshi, K., Visbal, E., & Haiman, Z. 2020, ARA&A, 58, 27
Jin, S., Daddi, E., Liu, D., et al. 2018, ApJ, 864, 56
Kartaltepe, J. S., Rose, C., Vanderhoof, B. N., et al. 2023, ApJL, 946, L15
Kellermann, K. I., Sramek, R., Schmidt, M., Shaffer, D. B., & Green, R. 1989, AJ, 98, 1195
Kocevski, D. D., Onoue, M., Inayoshi, K., et al. 2023, ApJL, 954, L4
Koekemoer, A. M., Aussel, H., Calzetti, D., et al. 2007, ApJS, 172, 196
Labbe, I., Greene, J. E., Bezanson, R., et al. 2023, arXiv:2306.07320
Lacy, M., Baum, S. A., Chandler, C. J., et al. 2020, PASP, 132, 035001
Laigle, C., McCracken, H. J., Ilbert, O., et al. 2016, ApJS, 224, 24
Larson, R. L., Finkelstein, S. L., Kocevski, D. D., et al. 2023, ApJL, 953, L29
Larson, R. L., Hutchison, T. A., Bagley, M., et al. 2023, ApJ, 958, 141
Liu, D., Daddi, E., Schinnerer, E., et al. 2021, ApJ, 909, 56
Liu, D., Lang, P., Magnelli, B., et al. 2019, ApJS, 244, 40
Maiolino, R., Scholtz, J., Curtis-Lake, E., et al. 2023, arXiv:2308.01230
Matsuoka, Y., Onoue, M., Iwasawa, K., et al. 2023, ApJL, 949, L42
Matthee, J., Naidu, R. P., Brammer, G., et al. 2023, arXiv:2306.05448
McKinney, W. 2010, in Proc. IX Python in Science Conf., ed. S. van der Walt & J. Millman (Austin, TX: SciPy), 51
Miley, G., & De Breuck, C. 2008, A&ARv, 15, 67
Mortlock, D. J., Warren, S. J., Venemans, B. P., et al. 2011, Natur, 474, 616
Mullaney, J. R., Alexander, D. M., Goulding, A. D., & Hickox, R. C. 2011, MNRAS, 414, 1082
Ni, Y., Di Matteo, T., Gilli, R., et al. 2020, MNRAS, 495, 2135
Onoue, M., Matsuoka, Y., Kashikawa, N., et al. 2021, ApJ, 919, 61
Pérez, F., & Granger, B. E. 2007, CSE, 9, 21
Polisensky, E., Richards, E., Clarke, T., Peters, W., & Kassim, N. 2019, in ASP Conf. Ser. 523, Astronomical Data Analysis Software and Systems XXVII, ed. P. J. Teuben et al. (San Francisco, CA: ASP), 441
Sanders, D. B., Salvato, M., Aussel, H., et al. 2007, ApJS, 172, 86
Saxena, A., Jagannathan, P., Röttgering, H. J. A., et al. 2018a, MNRAS, 475, 5041
Saxena, A., Marinello, M., Overzier, R. A., et al. 2018b, MNRAS, 480, 2733
Scoville, N., Aussel, H., Brusa, M., et al. 2007, ApJS, 172, 1
Shen, X., Hopkins, P. F., Faucher-Giguère, C.-A., et al. 2020, MNRAS, 495, 3252
Smolčić, V., Ciliegi, P., Jelić, V., et al. 2014, MNRAS, 443, 2590
Smolčić, V., Novak, M., Bondi, M., et al. 2017, A&A, 602, A1
Urry, C. M., & Padovani, P. 1995, PASP, 107, 803
Virtanen, P., Gommers, R., Oliphant, T. E., et al. 2020, NatMe, 17, 261
Vito, F., Brandt, W. N., Bauer, F. E., et al. 2019, A&A, 630, A118
Vito, F., Brandt, W. N., Yang, G., et al. 2018, MNRAS, 473, 2378
Wang, F., Yang, J., Fan, X., et al. 2021, ApJL, 907, L1
Weaver, J. R., Kauffmann, O. B., Ilbert, O., et al. 2022, ApJS, 258, 11
Yamashita, T., Nagao, T., Ikeda, H., et al. 2020, AJ, 160, 60